

Electron energy distribution functions in weakly ionized argon

S B Vrhovac, S B Radovanov, Z Lj Petrović and B M Jelenković

Institute of Physics, P.O. Box 86, 11080 Zemun, Beograd, Yugoslavia

Received 17 January 1991, in final form 28 August 1991

Abstract. In this paper we present measurements of the electron energy distribution functions (EEDF) for electrons in argon discharges at moderate and high E/N values (E being the electric field and N the gas density), for homogeneous electric fields and a low-current diffuse glow regime. Results were obtained for electric field to gas density ratios (E/N) from 500 Td to 50 kTd ($1 \text{ Td} = 10^{-21} \text{ V m}^2$). A multigridded energy analyser with a retarding grid potential was used to measure distribution functions of electrons sampled through an aperture in the anode. Experimental data are used to make a comparison with the two-term Boltzmann calculations for $E/N < 1 \text{ kTd}$, and the single-beam model predictions, normally used to model electron kinetics at high values of E/N .

1. Introduction

For electrons in equilibrium with an electric field, numerical techniques for calculating the electron energy distribution function (EEDF) have reached a high degree of accuracy (Lin *et al* 1979, Pitchford and Phelps 1982, Kitamori *et al* 1978, Segur *et al* 1983, Morgan and Penetrante 1990, Gibson 1970) which by far exceeds the accuracy of the available experimental techniques to obtain directly the EEDF.

At very high E/N values electrons are not in equilibrium with the electric field so the numerical techniques required for calculating their motion become increasingly complicated as they must include the effect of boundaries, and the transport coefficients are no longer properly defined, i.e. they become spatially dependent. Phelps *et al* (1987) have developed a single-beam model which was successfully applied to model electron kinetics at high E/N (Jelenković and Phelps 1987, Phelps and Jelenković 1988). Monte Carlo techniques (Braglia and Lowke 1979, Bhasavanich and Parker 1977, Kelly and Blevin 1989) are best suited to the study electron motion under these conditions but have been applied only in a very few situations.

Experimental techniques used to determine the EEDF in gas discharges and plasmas are either different applications of probes (Boyd and Twiddy 1959, Klage *et al* 1977, Amemya and Shimizu 1974, Barnes 1966) or sampling of electrons through apertures at the surface of the anode (Kenny and Craggs 1970) and subsequent analysis by the retarding potential energy analyser. Losee and Burch (1972) and Makabe *et al* (1977) have applied the latter technique to determine both the zeroth- (f_0) and the first-order (f_1) components in the EEDF expansion in spherical harmonics.

They have covered the range of moderate values of E/N assuming that at these E/N the distribution function is nearly spherically symmetric in the velocity space. The measurements of EEDF were criticized because they are in general performed close to a metallic boundary which may significantly alter the shape of the distribution function (Braglia *et al* 1984). However, at high E/N , non-equilibrium regions may take up a large part of the discharge gap (Kelly and Blevin 1989, Blevin *et al* 1987), and there is more justification to obtain the EEDF experimentally.

In this paper we present the measurements of EEDF in steady-state, self-sustained low-current Ar discharges for a wide range of E/N ($500 \text{ Td} < E/N < 50\,000 \text{ Td}$), and gas number density values ($1.6 \times 10^{22} > N > 3 \times 10^{21} \text{ m}^{-3}$). The measurements were done using the retarding potential difference technique. The main purpose of these measurements is to test the predictions of the single-beam model as applied by Phelps and Jelenković (1988). This work is relevant to models of electron motion in the cathode fall of glow discharges in rare gases (Gottscho *et al* 1988, Mitchell *et al* 1989, Sommerer and Lawler 1988, Boeuf 1990). Our data may also be used to determine scattering cross sections in conjunction with the measurements of excitation coefficients. To our knowledge there have been no previous measurements of the electron energy distribution function at the anode at very high E/N .

2. Experiment

Our apparatus is a two-section stainless-steel chamber consisting of a discharge section and an analysis section

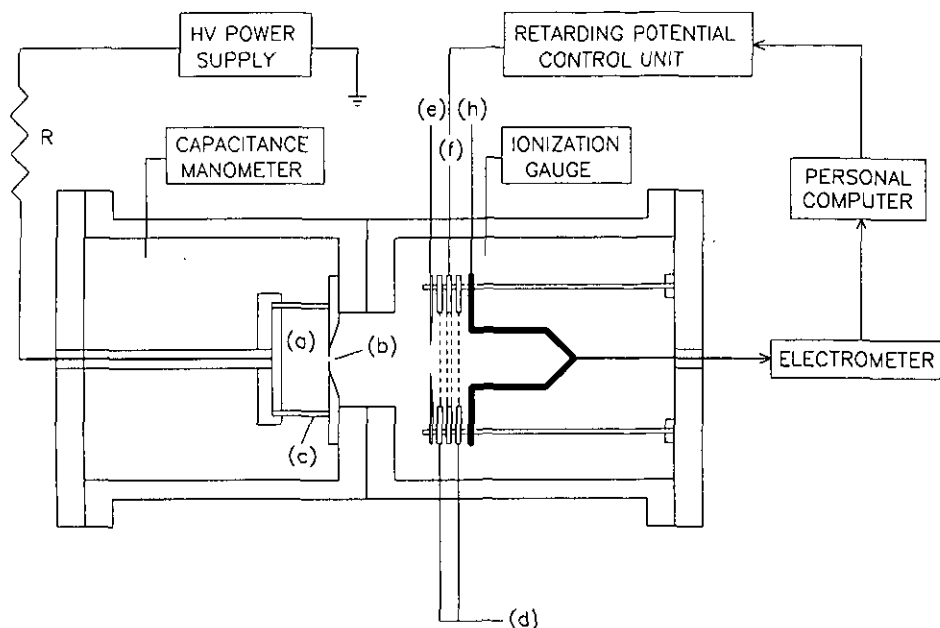


Figure 1. Schematic diagram of the discharge chamber and the analyser. (a) Discharge region, (b) aperture (grounded electrode), (c) quartz tubing, (d) shielding grids, (e) skimmer, (f) retarding grid; (h) Faraday cup; resistor, $R = 100 \text{ M}\Omega$.

(figure 1). The discharge was confined between the two parallel electrodes, with diameter 40 mm and spacing 20 mm, by placing the electrodes in a quartz cylinder.

The anode was made out of graphite to minimize the yield of backscattered and secondary electrons. The two sections of the vacuum chamber were connected through the sampling aperture on the grounded anode. Different diameters and thicknesses of the apertures were used. The results presented here were taken with diameters of 0.5 mm and 0.25 mm and thickness of 0.2 and 0.1 mm, respectively. Fitting of the electrodes in the cylinder is tight enough to prevent the long-path breakdown but it gives very little resistance to the gas flow so that pressure could be measured accurately outside the glass envelope. The pressure in the discharge region was between 0.1 and 0.6 Torr and in the differentially pumped analyser section between 10^{-6} and 10^{-4} Torr. Research-purity argon was used without further purification.

It was possible to operate the discharge to the left and to the right of the minimum of the Paschen curve, in a wide range of E/N , between 500 Td and 50 kTd. The Paschen curve was reproducible. The discharge was stabilized by using a large resistor in series with the discharge. The discharge current was typically 2–5 μA , thus the electric field between electrodes was uniform and the breakdown voltage was independent of the current.

We have made measurements using a retarding analyser with a set of three or four grids with 90% transmission meshes. The retarding voltage was applied to the middle grid(s), while two outside grids were grounded. A skimmer with an open cone of 12.7 mm diameter was mounted at a distance of 3.5 mm from the first grid to limit the incident angle of the sampled

electrons to 7° . The distance between two retarding grids was 0.6 mm, and the distance between the grounded and retarding grid was 3.5 mm. The electrons were collected by a Faraday cup. This was a graphite cylinder with a hole of diameter 25 mm and depth 80 mm. The distance between the Faraday cup and the grounded grid next to it was 0.4 mm.

As established already (Taylor 1969), the set-up with the double retarding grids reduces the effect of local variations in potential in the vicinity of the retarding grid, increasing the energy resolution in comparison to the single-grid system. The electrons that originated at the cathode and pass the gap without collisions have a narrow energy distribution at the anode at $E/N \geq 25 \text{ kTd}$. From the energy peak of the cathode beam electrons we were able to determine the energy resolution of our detection system, defined as $\Delta E/E$, where ΔE is the full width at half maximum of the peak, and E is the energy of the beam, i.e. the total gap voltage. For the system with two retarding grids and $E/N \geq 25 \text{ kTd}$ the resolution was found to be independent of E/N , or beam energy, and to be around 2.5×10^{-2} .

3. Theory of the experiment

We shall outline here briefly the type of distribution functions that can be obtained in an experimental approach like ours, and some problems related to this technique. The energy of electrons at the anode, and therefore the measured electron current versus retarding voltage, is determined by the values of E/N and the product Nd , where d is the electrode spacing.

At high E/N the contribution of backscattered electrons from the anode to the lower-energy part of the distribution function can be significant. But, the electron current at a certain retarding voltage also depends on the electron angular distribution function and the solid angle of the retarding field analyser. Moreover, the result can be affected by the collection efficiency of the detector, the electric field distortion near the aperture, and by electron collisions with the residual gas behind the aperture. There is also the effect of finite thickness of the aperture, e.g. a fraction of the electrons which pass through the orifice may strike the inner wall of the orifice. Such an effect makes the effective area of the aperture smaller for higher incident angles and is proportional to the ratio of the aperture thickness. Therefore the electron current that emerges from the discharge through the aperture and which has been measured by the Faraday cup I_c is given by the following expression (Losee and Burch 1972)

$$I_c(U_R) = qS\tau \int_{v_R}^{+\infty} dv_z v_z T(v_z) \times \iint_{(D(v_z))} dv_x dv_y \eta(\xi, \Theta) f(0, v) D_{\xi, \Omega}(\Theta, v_z) \quad (1)$$

where $v_R = (2qU_R/m)^{1/2}$, q is electron charge, S is the area of the cathode aperture, τ is the transmission coefficient including all grids, $f(0, v)$ is the electron velocity distribution function at the anode ($z = 0$); $T(v_z)$ is the collection efficiency of the Faraday cup, i.e. the ratio of the electrons with velocity v_z passing into the Faraday cup to those being collected, $\eta(\xi, \Theta)$ is the ratio of the effective area of the aperture for different incident angles Θ , to the actual area of the aperture, and $D_{\xi, \Omega}(\Theta, v_z)$ is the electric field distortion function, i.e. the fraction of electrons collected into the solid angle of the analyser after passing the aperture to the total number of electrons incident on the aperture. The distortion function depends on the ratio of the thickness and the diameter of the aperture ξ , solid angle Ω , and electric field present in the discharge E ; $D(v_z)$ in the double integral limits is basically an area of the circle in the (v_x, v_y) velocity frame, with the radius $v_z \tan \Theta_m$, where Θ_m is the maximum incident angle of electrons, determined by the solid angle of the detector.

The shape of our Faraday cup is such as to minimize the fraction of those electrons which can escape from the cup. We did not measure $T(v_z)$ independently, since some of our measurements when the grid next to the Faraday cup was the retarding grid (which makes the suppression field for the electrons escaping from Faraday cup), gave the same results as when this grid was grounded. Therefore we will assume that $T(v_z) = 1$.

The fraction of ions which pass through the aperture within the solid angle of our detection system and which do not hit the walls of the aperture depend on the incident angle of the electron and on ξ . Since in

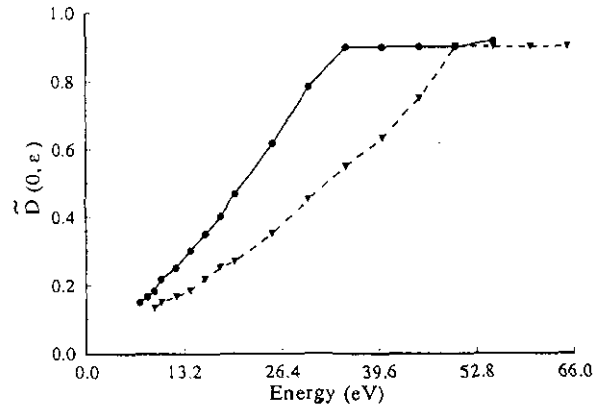


Figure 2. The variation of $\bar{D}_{\xi, \Omega}(\epsilon)$, the electric field distortion function, with incident electron energy at anode for aperture diameter of 0.3 mm and electric field of 800 V cm^{-1} (full curve, $E/N = 30 \text{ kTd}$) and 1400 V cm^{-1} (broken curve, $E/N = 50 \text{ kTd}$).

our experiments the solid angle 7° and ξ was 0.25 we can set $\eta = 1$ (Liu *et al* 1990).

The defocusing effect on electrons passing through the aperture was analysed experimentally using a different aperture diameter and theoretically using the calculation procedure given by the program 'Simion' (Dahl 1985). The calculated value of $\bar{D}_{\xi, \Omega}(\Theta, \epsilon)$, for an aperture of 0.3 mm diameter, and for $\xi = 0.25$ and $\Omega = 7^\circ$, and for two values of the electric fields in the discharge, of 800 V cm^{-1} ($E/N = 30 \text{ kTd}$), and of 1400 V cm^{-1} ($E/N = 50 \text{ kTd}$), versus electron energy, is shown in figure 2. The calculations were done assuming the electrons incident on the anode are normal to it, $\Theta = 0$. As shown in figure 2 such calculations allow us to determine the minimum electron energy so that it can pass the field-distorted region without deflection. Both experiment and calculation have shown that this energy is lower if the size of the aperture is smaller. It turns out that the energy region where the effect of the field exists overlaps with the region where the contribution to the energy distribution function from the secondary electrons ejected from the anode is becoming significant.

If we now define $h(v_z)$ to be

$$h(v_z) = \int_0^{2\pi} d\varphi \int_0^{v \tan \Theta} v_\perp f(v) dv_\perp \quad (2)$$

where $v_\perp = (v_x^2 + v_y^2)^{1/2}$, then it follows from equation (1), for the energy distribution function measured in our experiments

$$h(v_z) = -\frac{m}{q^2 \tau S} \frac{1}{D_{\xi, \Omega}(0, v_z)} \frac{dI_c(U_R)}{dU_R} \quad (3)$$

where $U_R = (mv_z^2/2q)$. $h(v_z)$ is the distribution function of the axial component of the electron velocity, i.e. $h(v_z) dv_z$ represents the number of electrons emerging from the discharge with axial components of the velocity within the interval $(v_z, v_z + dv_z)$, and whose transverse velocity components are such that the

relation $(v_x^2 + v_y^2)^{1/2} < v_z \tan \Theta_m$ holds. In gas discharges at high electric field to gas density ratios the electron velocity distribution function is highly anisotropic, with most electrons moving along the field lines. Then the measured distribution function $h(v_z)$ becomes the reduced distribution function $\tilde{f}(v_z) = \int dv_x \int dv_y f(v)$. There is an electron energy distribution function $F(\varepsilon)$, related to $h(v_z)$ by the relation $F(\varepsilon) d\varepsilon = h(v_z) dv_z$, with $\varepsilon = (mv_z^2/2)$. Since dI_c/dU_R is determined in terms of U_R , or electron energy ε , we obtain $F(\varepsilon)$ versus ε directly from the following equation

$$F(\varepsilon) = -\frac{(m/2)^{1/2}}{q^2 \tau S} \frac{1}{(\varepsilon_z)^{1/2} \bar{D}_{\xi, \Omega}(0, \varepsilon_z)} \frac{dI_c(U_R)}{dU_R}. \quad (4)$$

The experimental mean energy of electrons $\langle \varepsilon \rangle_c$ was obtained from the relation

$$\langle \varepsilon \rangle_c = \frac{\int F(\varepsilon) \varepsilon d\varepsilon}{\int F(\varepsilon) d\varepsilon}. \quad (5)$$

The values of $\langle \varepsilon \rangle_c$ for different E/N will be compared with calculations of $\langle \varepsilon \rangle_c$.

4. Calculation of the mean electron energy

Our measured mean electron energies at the anode, for the lowest E/N in the experiment ($E/N < 1$ kTd) were compared with our calculations using the two-term code of the Boltzmann equation of Yoshida *et al* (1983) with the available argon cross sections (Tachibana 1986).

The experimental measurement of the mean electron energy at the anode at high E/N discharges is an additional test of the single-beam model. The model was first discussed by Phelps *et al* (1987) and since then has been applied to a uniform electric field (Jelenković and Phelps 1987, Gylis *et al* 1989, Stojanović *et al* 1990) and to a non-uniform electric field of DC and RF glow discharges (Gottscho *et al* 1988, 1989, Mitchell *et al* 1989). The model was able to predict very well the spatial variation of light and the transient behaviour of charge carried by electrons and ions in high- E/N low-current discharges. It also predicts the spatial variation and magnitude of the ion density, the existence of field reversal, and a charge double layer in glow discharges. But the single-beam model overestimates the ionization rate in the negative glow and fails to accurately predict the position of the field reversal. Boeuf (1990) extended the idea towards a two-group electron model that treats the low-energy electrons in the negative glow using transport equations.

4.1. Single-beam model

The electron kinetics at high E/N was calculated using the single-beam, energy-balance model. The electron-velocity distribution function is that of the mono-energetic beam moving along the electric field, i.e.

$f(v, \Theta, z) = n_c(z) \delta(v - u(z)) \delta(\Theta)$, where u is the velocity of the beam at z . The integration of the first three velocity moments of the steady-state Boltzmann equation with the assumed distribution function yields the particle number, momentum and energy-balance equations. The electron density was eliminated by combining number balance with either momentum or energy-balance equations. The equation describing the electron beam velocity (or energy) was next obtained. Phelps *et al* (1987) have found that beam models based on the energy-balance model agree better with experiment and with more detailed models than beam models based on momentum balance. The equation of the spatial growth of the electron beam energy ε is then given by

$$\frac{d\varepsilon}{d\xi} = \frac{eE}{n} - \sum_{k,i} \varepsilon_m Q_c^m(\varepsilon) - \varepsilon \left(Q_c^i(\varepsilon) + \frac{\alpha_p^i \Gamma_p(\xi)}{n \Gamma_c(\xi)} + \frac{\alpha_f^i \Gamma_f(\xi)}{n \Gamma_c(\xi)} \right). \quad (6)$$

The first term includes the energy gain from the field while the second includes the energy lost in inelastic collisions, ε_m and Q_c^m being threshold energy and the cross section for the inelastic process, respectively. Since all electrons of the beam at position z have the same energy, the third term includes the energy required to raise the energy of new electrons produced by electron, ion and fast neutral ionization to the beam energy. $\alpha_{p,n}/N$ and $\Gamma_{p,n}$ are spatial ionization coefficients for ions (p) and neutrals (n), and ion and fast neutral flux, respectively. The equation for the spatial variation of the electron beam energy was coupled with the differential equations for the spatial growth of the electron flux, Γ_c , and the equations for the ion and fast neutral flux, Γ_p and Γ_n . In the ion continuity equation new ions are produced in ionizing collisions by electrons, ions and fast atoms, while the continuity equation for the fast atom flux includes the production in charge transfer collisions and loss by any collision process, because the relevant group of atoms is that with high energies, above the threshold for ionization.

As for the electron energy loss function and ionization, we have used an analytical approximation of the cross sections given by Phelps *et al* (1987). The ionization coefficients for heavy particles were calculated assuming that they are in equilibrium with the Maxwellian energy distribution function in the direction of the field. We used their cross sections for charge transfer, for the ionization by ions, and for ionization by fast Ar.

A fraction of the beam of energetic electrons is reflected back from the anode. Papers dealing with carbon surfaces (Sternglass 1954, Darlington and Cosslett 1972, Verna 1977) present the backscattering coefficient as a function of incident electron energy, the energy distribution of reflected electrons and the variation of the coefficient with the incident angle. The results differ widely for the backscattering coefficient at electron incident energies below several keV. Working

with colloidal graphite Sternglass (1954) found a very low value of 0.08 and very small variation of backscattered coefficient with electron energy, while results obtained by Darlington and Cosslett (1972), for mechanically polished carbon, show a decrease of the coefficient with electron energy, from about 0.5 at 500 eV to 0.25 at 1 keV. Such differences suggest a strong variation of the backscattering coefficient with the surface condition, and yet there are no measurements that we know of for the graphite surface exposed to discharge. On the other hand, different authors show much better agreement on the energy distribution function of backscattered electrons, saying that it is a relatively flat function and the average energy is around half of the incident electron energy.

The high-energy electrons can also eject secondary electrons. These are low-energy electrons in comparison with backscattered electrons, with an energy distribution function peaking at about 10 eV and with a negligible fraction above 50 eV. The measurements of the secondary-electron yield of the graphite surface were done for clean graphite and graphite exposed to JET tokamak plasmas (Woods *et al* 1985, 1987). The yield at normal incidence increases with energy up to a maximum at around 350 eV and then decreases slowly. The maximum for clean graphite is around 0.7 while for the graphite taken from a tokamak it is close to unity.

Since our results for the measured electron energy distribution function at E/N greater than 6 kTd have shown a very high fraction of low-energy electrons, with average electron energy at the anode far below that calculated from the single-beam model, we did the calculations of mean electron energy at the anode with the modified single-beam model to include beams of backscattered electrons. The first beam of backscattered electrons starts at a distance z_1 from the anode that the electrons can reach after being reflected from the anode, with energy equal to half of the energy of the primary beam (both the energy and the current of the primary beam were calculated from the single-beam model assuming no backscattering) and then travelling against the field. The initial value of the current of backscattered electrons at the position z_1 was taken as a product of the backscattering coefficient and the independently calculated multiplication of the electron beam at the same E/N and for the distance z_1 . A fraction of the new beam will also be reflected at the anode contributing to the second beam of backscattered electrons. The starting position z_1 , and the initial value of the current of the beam, were determined from the energy and current of the first beam of backscattered electrons at the anode. The contribution of the next backscattered beam to the electron current at the anode was negligible. It is the presence of backscattered electrons rather than the ionization by them that is important. At $E/N = 30$ kTd, for example, the increase of ionization due to the presence of backscattered electrons is about 20%. This is in accordance with the value that Phelps and Jelenković

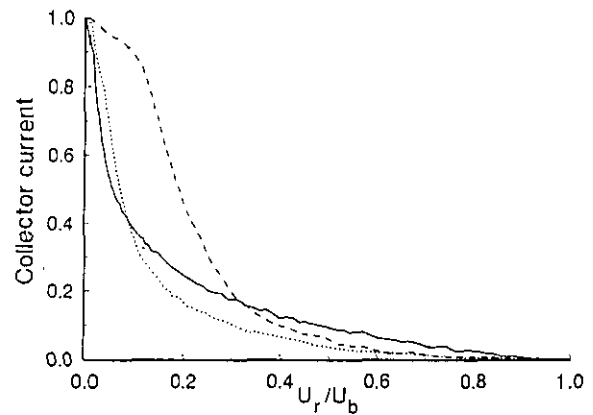


Figure 3. Electron current of the Faraday cup as a function of the retarding potential for moderate values of E/N : 0.8 kTd (broken curve, $U = 220$ V, $p = 800$ mTorr); 2 kTd (dotted curve, $U = 280$ V, $p = 230$ mTorr); and 4 kTd (full curve, $U = 400$ V, $p = 165$ mTorr) (U is discharge voltage and p is gas pressure).

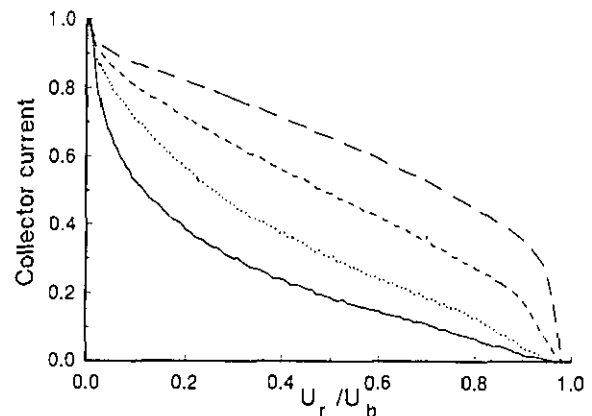


Figure 4. Electron current of the Faraday cup as a function of the retarding potential for high E/N : 6 kTd (full curve, $U = 510$ V, $p = 145$ mTorr); 12 kTd (dotted curve, $U = 870$ V, $p = 120$ mTorr); 20 kTd (short broken curve, $U = 1200$ V, $p = 102$ mTorr); 50 kTd (long broken curve, $U = 2600$ V, $p = 84$ mTorr); values in parentheses are corresponding discharge voltages and pressures.

(1988) had to use as a yield of ions per electron striking the anode to fit experimental values of discharge voltage versus Nd . Finally, a beam due to low-energy secondary electrons was added to the incoming beams, assuming no ionization was made by secondary electrons, and with the variation of the yield of secondary electrons with energy of incoming electrons taken from Woods *et al* (1987).

5. Results and discussion

Our measurements were done for a wide range of E/N values, from moderate, where electrons reach equilibrium with the field at different distances from the cathode, to high, where most of the electrons behave as if in free-fall. Different behaviours of electrons at different E/N can be seen in figures 3 and 4. The figures show dependence of electron currents

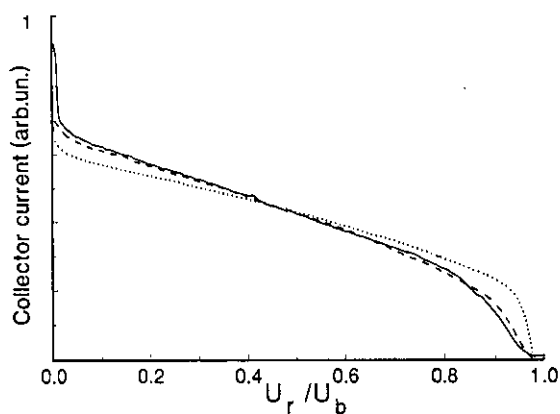


Figure 5. Variation of the electron current of the Faraday cup using the single retarding grid and 0.5 diameter aperture on a graphite anode (broken curve), the single retarding grid on a stainless steel anode (full curve) and the double retarding grid and the 0.3 mm aperture on a graphite anode (dotted curve).

measured by the Faraday cup as a function of the retarding potential U_R at 800 Td to 50 kTd. We grouped discharges as those below and above around 6 kTd, because of the different shape of I_c versus U_R , i.e. different shapes of energy distribution function. And we can say that the terms moderate and high, as defined at the beginning of these sections, are for discharges at E/N below and above 6 kTd, respectively. From the exponential growth of the light emission from Ar discharges (an indication that electrons reach the equilibrium) Phelps and Jelenković (1988) found ionization coefficients that agree well with the beam model (Phelps *et al* 1987) at E/N up to around 6 kTd.

As we have pointed out already, the results of our measurements are affected by electron reflection and ejection from the anode surface. The technique itself imposes additional problems that have to be taken into account. The data presented in figures 3 and 4, and analysed and discussed in terms of energy distribution functions later, were obtained using a 0.3 mm aperture on the graphite anode, and the double retarding grid in the energy analyser. In order to estimate the effect of electric field distortion at the aperture and the pressure effect in the analysis region on the electrons passing to the analyser we have also made measurements with different aperture diameters. The broken curve of I_c versus U_R at 50 kTd presented in figure 5, was obtained with 0.5 mm diameter of the aperture on the graphite anode, and with a single retarding grid analyser. The results obtained with double grid and 0.3 mm aperture are shown by the dotted curve. One can see that the double retarding grid gives the higher energy resolution at high retarding voltages, and that a smaller aperture (and smaller field effect, as predicted by 'Simion' calculations) gives a stronger variation of I_c at low retarding voltages due to the fact that more low-energy electrons are now passing towards the grids of the analyser.

Another problem related to this type of measurement is the pressure effect. Although the gas density changes very rapidly behind the aperture, reaching the vacuum of the analysis region at a distance equal to the aperture diameter (Coburn and Kay 1971, Gustafson and Kiel 1963), we really do not know whether or not the electron collisions behind the aperture are important to the low-energy part of the distribution function. There are two types of pressure effects: influence of the static pressure in the analysis region and also of the local pressure on the effusing neutral particles. The former effect is not important since the results do not change after slightly closing the valve to the vacuum pump, changing the static pressure in the chamber by nearly a factor of 10. The fair agreement between measured and calculated mean electron energy at the lowest E/N (and highest pressure) of our experiment can be an indication that the total pressure effect is not important, particularly at high E/N because of the lower pressure in the discharge region.

The full curve shown in figure 5 is for the stainless-steel anode. The curves in figure 5 are normalized at half value of the discharge voltage. There is a remarkable difference at very low retarding voltages, below 50 eV, which may be due to a higher yield of both secondary electrons ejected and primary electrons reflected back from the stainless-steel anode. We think that the higher fraction of lower electron energy, obtained with stainless steel, relative to that obtained with graphite is a combined effect of both secondary and backscattered electrons. A similar effect was noted by Jelenković and Phelps (1987) from the light emission in N_2 discharges at very high E/N .

Current-voltage curves like those shown in figures 3 and 4 were smoothed by a polynomial fit and then were differentiated according to equation (4) to obtain the energy distribution functions $F(\epsilon)$. The experimental mean energy of electrons at the anode was calculated using equation (4), and it is the $\langle \epsilon \rangle_c$ that we will compare with results from Boltzmann calculations (for $E/N \leq 1$ kTd) and the beam model (for $E/N \geq 6$ kTd).

5.1. Moderate E/N

The results for the effective distribution function $F(\epsilon)$ are presented in figure 6 for two moderate values of E/N . In all cases, at those E/N , we have a monotonically decreasing distribution function, similar to the results of Losee and Burch (1972) and Makabe *et al* (1977) at $E/N \leq 500$ Td. We did not perform the calculations of the components of the EEDF, f_0 and f_1 , from the measured I_c-U_R dependence as they did, since our geometry did not allow us to perform the deconvolution accurately.

At values of $E/N = 550$ Td ionization is expected to be by the electrons that reach collisional equilibrium with the electric field and the gas at distances short in comparison with the electrode separation. Secondary electrons from the ionization processes in the gap are

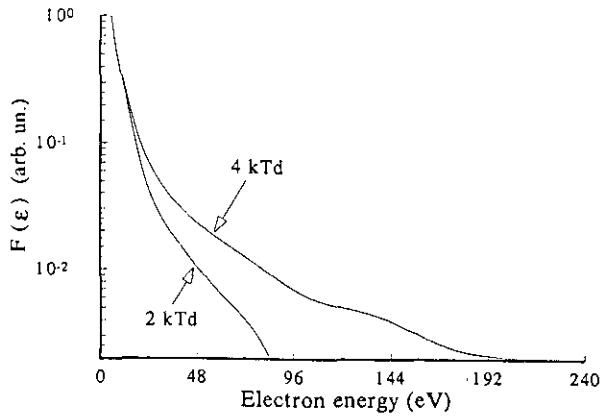


Figure 6. Electron energy distribution function, as discussed in text, versus electron energy for moderate values of E/N , 2 and 4 kTd.

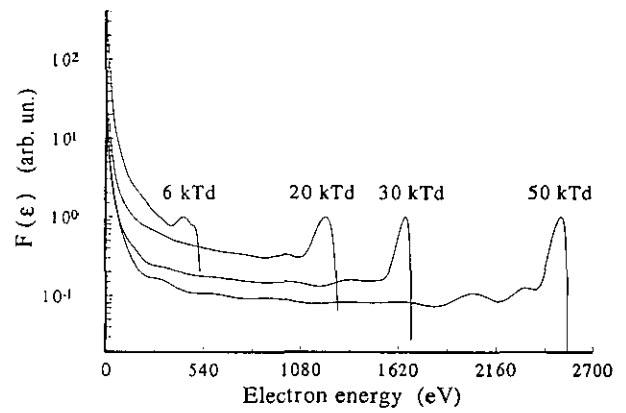


Figure 7. Measured electron energy distribution function for high E/N , 6 kTd, 20 kTd, 30 kTd and 50 kTd. The data are normalized at the maximum values of the high-energy peak.

Table 1.

E/N (kTd)	U (V)	$\langle \epsilon \rangle_e$ (eV)	$\langle \epsilon \rangle_c$ (eV)
0.55	225	8.2	9.8
1	230	9	13

expected to reach equilibrium also. The results of the experimental mean electron energy $\langle \epsilon \rangle_e$ are therefore compared with the mean electron energy $\langle \epsilon \rangle_c$ calculated from our Boltzmann calculations of electron velocity distribution function. The results for 550 kTd and also for 1 kTd are shown in table 1. There is relatively good agreement for 550 kTd and big discrepancy for 1 kTd. The Boltzmann calculations may not be appropriate for 1 kTd when electrons reach equilibrium at a larger distance from the cathode, at nearly half of the discharge gap.

At the upper limit of moderate values of E/N the electron ionization still dominates through the gap. But as has been shown from the spatial variation of the optical emission at 6 kTd by Phelps and Jelenković (1988), the electrons reach equilibrium only after travelling two-thirds of the discharge gap. The fraction of primary electrons that arrive at the anode without collisions was estimated to be less than 10^{-3} (using the energy-loss cross section as given by Phelps and Jelenković (1988)) and therefore cannot be seen in our experimental distribution function due to the limited detection sensitivity. The calculations done by a single-beam model for 6 kTd (not shown here) suggest that the ionization by fast atoms is small compared with electron ionization but cannot be neglected in the vicinity of the cathode.

5.2. High E/N region

The measured electron energy distribution functions $F(\epsilon)$ at $E/N \geq 10$ kTd are shown in figure 7. The gas pressures corresponding to particular E/N are given in

the figure captions, while one can read the discharge voltages from figure 7 as a value where $F(\epsilon)$ falls to zero. Characteristics of the electron energy distribution functions at high E/N values are a high fraction of very-low-energy electrons, a plateau extending almost to the discharge voltage, followed either by a sharp drop to zero (below 10 kTd), or a maximum (above 10 kTd). The peak is at the discharge voltage and is due to primary or runaway electrons which are emitted from the cathode and reach the anode without collisions. As expected, the fraction of beam electrons increases with increasing E/N value.

Table 2 gives the results of measured mean energy $\langle \epsilon \rangle_e$ and calculated beam energy $\langle \epsilon \rangle_c$ at the anode. The first two columns on the left, with superscript T, are mean energies of all electrons arriving at the anode. Values for the $\langle \epsilon \rangle_e^T$ were calculated using the single-beam model with the addition of beams of back-scattered electrons. The values for secondary-electron emission coefficients γ at different E/N , were obtained from γ s for different energies of primary and back-scattered beams and their relative contribution to the total electron current at the anode (Woods *et al* 1987). The values of backscattered coefficients η , shown also in parentheses, are average values for different energies of electron beams at every E/N , taken to have as good an agreement as possible with the experiment, and at the same time to be in the interval of published values for η for graphite.

The additional test of the single-beam model, i.e. how well it describes the behaviour of primary electrons, is also presented in table 2. The two right-most columns, $\langle \epsilon \rangle_e^P$ and $\langle \epsilon \rangle_c^P$, are mean energies of primary electron beams, calculated from the single-beam model assuming no secondary and backscattered electrons, and calculated from equation (5), respectively. The experimental value $\langle \epsilon \rangle_e^P$ was obtained with the low integration limits in equation (5) taken at the energy at which the plateau begins.

The results shown in table 2 for calculated values $\langle \epsilon \rangle_c$ were obtained assuming ionization by electrons,

Table 2.

E/N (kTd)	Nd (10^{-19} m^{-2})	$\langle \epsilon \rangle_e^T$ (eV)	$\langle \epsilon \rangle_c^T$ (eV)	$\langle \epsilon \rangle_e^P$ (eV)	$\langle \epsilon \rangle_c^P$ (eV)
6	8.7	65 ($\gamma = 0.65, \eta = 0.5$)	100		
12	7.2	170 (0.6, 0.45)	190		
20	6.1	360 (0.58, 0.4)	390	728	720
30	5.6	480 (0.56, 0.4)	530	1040	1100
50	5.0	780 (0.55, 0.4)	860	1700	1900

ions and fast neutrals. The single-beam model calculations have shown a very large flux of neutrals, which at 50 kTd, for example, exceeds the ion flux by a factor of six. The ionization by electrons at high E/N is significant only in the anode half of the discharge gap. Therefore ionization by neutrals strongly affects the spatial variation of the apparent ionization coefficient (Phelps and Jelenković 1988) by increasing the electron multiplication in the gap. The low-energy electrons are then expected to be more abundant in the energy distribution function. The results of $\langle \epsilon \rangle_c$ by the single-beam model when heavy particles were not taken as a source of new electrons gave a higher mean electron energy, about 300 eV at 50 kTd, and 55 eV at 12 kTd.

As one can see from figure 7, for 12 kTd a relatively small number of electrons ejected from the cathode can cross the gap without any collisions. This is in contrast to the result of Bhasavanich and Parker (1977) who have shown by Monte Carlo calculations that most of the electrons arrive at the anode with the full gap energy. The discrepancy may be due to the fact that these authors have omitted ionization by heavy particles.

From table 2, i.e. from the comparison between the experimental and calculated values of mean electron energy, it can be established that the low-energy part of the electron energy distribution function at high E/N is determined by the flux of backscattered electrons (and much less by multiplication by backscattered electrons) and the flux of secondary electrons. This seems to be so also for $6 \text{ kTd} < E/N < 12 \text{ kTd}$, although at those E/N electron ionization is still dominant.

6. Conclusion

The experiments and calculations presented in this paper give the results for the electron behaviour for moderate E/N where most of the electrons at the anode are in collisional equilibrium ($500 \text{ Td} < E/N < 6 \text{ kTd}$), to high E/N values where electrons normally reach equilibrium far from the cathode ($6 \text{ kTd} < E/N$

$< 12 \text{ kTd}$), or when electrons with fewer or no collisions start to dominate the high portion of the electron energy distribution function ($E/N > 12 \text{ kTd}$).

Our measurements of the electron energy distribution function and of the electron mean energy at the anode were done using the retarding potential technique. This technique has to be used carefully since results can be affected by different effects. The good agreement obtained at 550 Td, the lowest E/N and the highest pressure of the experiment, with calculations done using the Boltzmann equation, can be regarded as an indication of a small pressure effect in our measurements. For the other effects present we seem to know how to calculate, or at least how to estimate, their effect.

Comparison was made between the experimental and calculated values of electron mean energy at the anode. The calculations for $E/N \leq 1 \text{ kTd}$ were done using the Boltzmann calculations of the electron energy distribution function, and for $E/N \geq 6 \text{ kTd}$ using the single-beam model. The results and such comparisons have shown the changes of electron behaviour, and the increasing effect of backscattered electrons from the anode as E/N increases. The electron behaviour changes from equilibrium at 550 Td, to highly non-equilibrium at 50 kTd, when around 15% of electrons released from the cathode reach the anode without collisions in the gap. As E/N is increased from low values, we have found that the agreement between measured and calculated values, using Boltzmann calculations, of mean energy was not good even at 1 kTd. Also, the single-beam model gave a much higher mean energy of electrons arriving at the anode than did measurements, below 6 kTd. Both types of calculation did not work well in this transient region of moderate E/N values because electrons, which are the main source of ionization there, are not coming into equilibrium in distances short enough for Boltzmann calculations, and yet are still coming into equilibrium at large distances, when the electron energy distribution function cannot be described by a mono-energetic beam as in the single-beam model.

The single-beam model predicts that above 10 kTd the ionization by fast neutrals is more important in

the cathode end of the discharge than ionization by electrons. The values for mean electron energies of primary electrons only at the anode, obtained from experiment and calculated with the ionization by ions and neutrals using a single-beam model, are in much better agreement than when the heavy-particle effect is taken out. For example, the primary electron beam energy at the anode, for $E/N = 50$ kTd, is about 300 eV higher than shown in table 2 if ionization by those particles was not included.

The measurements with different anode materials having different coefficients for secondary and back-scattered electrons, and the comparison between experimental results and results of the single-beam model, showed the strong effect of backscattering and secondary electrons on the low part of the electron energy distribution function. The main impact on the energy distribution function is from backscattered electrons themselves, rather than from ionization by back-scattered electrons.

Therefore we can conclude that a simple single-beam model can well represent the behaviour of electrons in the primary beam from the cathode in high E/N gas discharges. With the inclusion of beams of backscattering electrons from the anode the model can also predict very well the mean electron energy of all electrons at the anode.

Acknowledgments

The authors are grateful to JILA, University of Colorado, and the National Institute of Standards and Technology for loaning us some of the equipment used in this project and to A V Phelps for very useful discussions. The work presented in this paper was partially supported by the Science Foundation of Serbia, by USA–Yugoslav projects NIST JF 924 and 926 and IAEA project No 5950/RB.

References

- Amemya H and Shimizu K 1974 *Japan. J. Appl. Phys.* **13** 1035
- Barnes B T 1966 *J. Appl. Phys.* **37** 2679
- Bhasavanich D and Parker A B 1977 *Proc. R. Soc. A* **358** 385
- Blevin H A, Brennan M J and Kelly L J 1987 *Int. Conf. on Phenomena in Ionized Gases (XVIII Int. Conf., Swansea, July 1987)* ed W T Williams vol 1 Contributed Papers p 92
- Boeuf J P 1990 *The Physics and Application of Pseudosparks* ed M A Gundersen and G Schaefer (New York: Plenum) in press
- Boyd R L F and Twiddy N D 1959 *Proc. R. Soc. A* **250** 53
- Braglia G L and Lowke J J 1979 *J. Phys. D: Appl. Phys.* **12** 1831
- Braglia G L, Romano L and Diligenti M 1984 *Nuovo Cimento* **79** B 93
- Coburn J W and Kay E 1971 *J. Vac. Sci. Technol.* **8** 738
- Dahl D A 1985 *Simion PC* (Idaho Falls, ID: EG&G Idaho)
- Darlington E H and Cosslett V E 1972 *J. Phys. D: Appl. Phys.* **5** 1969
- Gibson D K 1970 *Aust. J. Phys.* **23** 683
- Gottscho R A, Mitchell A, Scheller G R and Chan Y Y 1989 *Phys. Rev. A* **40** 6407
- Gottscho R A, Mitchell A, Scheller G R and Schryer N L 1988 *J. Electrochem. Soc.* **1** 88
- Gustafson W A and Kiel R E 1963 *Phys. Fluids, Research Notes* 472
- Gylis V T, Jelenković B M and Phelps A V 1989 *J. Appl. Phys.* **65** 3369
- Jelenković B M and Phelps A V 1987 *Phys. Rev. A* **36** 5310
- Kelly L J and Blevin H A 1989 *Proc. XIX ICPIG (Belgrade)* Contributed Papers (Belgrade: University of Belgrade) p 893
- Kenny T E and Craggs J D 1970 *J. Phys. B: At. Mol. Phys.* **3** 251
- Kitamori K, Tagashira H and Sakai Y 1978 *J. Phys. D: Appl. Phys.* **11** 283
- Klagge S, Pfau S, Rezacova V and Winkler R 1977 *Beitr. Plasmaphys.* **17** 237
- Lin S L, Robson R E and Mason E A 1979 *J. Chem. Phys.* **71** 3483
- Liu J, Huppert G L and Sawin H H 1990 *J. Appl. Phys.* **68** 3916
- Losee J R and Burch D S 1972 *Phys. Rev. A* **6** 1652
- Makabe T, Goto T and Mori T 1977 *J. Phys. D: Appl. Phys.* **10** 1781
- Mitchell A, Scheller G R, Gottscho R and Graves D B 1989 *Phys. Rev. A* **40** 5199
- Morgan W L and Penetrante B M 1990 *Comput. Phys. Commun.* **58** 127
- Phelps A V and Jelenković B M 1988 *Phys. Rev. A* **38** 2975
- Phelps A V, Jelenković B M and Pitchford L C 1987 *Phys. Rev. A* **36** 5327
- Pitchford L C and Phelps A V 1982 *Phys. Rev. A* **25** 540
- Segur P, Bordage M, Belenguer J and Yousfi M 1983 *J. Comput. Phys.* **50** 116
- Sommerer T J and Lawler J E 1988 *J. Appl. Phys.* **64** 1775
- Sternglass E J 1954 *Phys. Rev.* **95** 345
- Stojanović V, Božin J, Petrović Z Lj and Jelenković B M 1990 *Phys. Rev. A* **42** 4983
- Tachibana K 1986 *Phys. Rev. A* **34** 1007
- Taylor N J 1969 *Rev. Sci. Instrum.* **40** 792
- Verna R L 1977 *J. Phys. D: Appl. Phys.* **10** 1167
- Woods M E, Hopkins B J, Matthews G F, McCracken G M, Sewl P M and Fahrang H 1987 *J. Phys. D: Appl. Phys.* **20** 1136
- Woods M E, Hopkins B J and McCracken G M 1985 *Surf. Sci.* **162** 928
- Yoshida S, Phelps A V and Pitchford L C 1983 *Phys. Rev. A* **27** 2858